Magnetic helicity in fast dynamos

Andrew D. Gilbert,
School of Mathematical Sciences,
University of Exeter,
Exeter EX4 4QE, U.K.

Summary

The behaviour of magnetic helicity in kinematic dynamos at large magnetic Reynolds number is considered. Hughes, Cattaneo & Kim (1996) observe that the relative helicity tends to zero in the limit of large magnetic Reynolds number. This paper gives upper bounds on the helicity, by relating the helicity spectrum to the energy spectrum. These bounds are confirmed by numerical simulation and the distribution of helicity over scales is considered. Although it is found that the total helicity becomes small in the limit of high conductivity, there can remain significant, but cancelling, helicity at large and small scales of the field. This is illustrated by considering the evolution of helicity in the stretch–twist–fold dynamo picture.

Key words:

Magnetohydrodynamics, Magnetic fields.

Submitted to Mon. Not. R. Astro. Soc., March 2001.

1. Introduction

Magnetic fields in the Sun, planets and galaxies are generally believed to be generated by dynamo processes, governed by the magnetic induction equation

$$\partial_t \mathbf{B} = \nabla \times (\mathbf{u} \times \mathbf{B}) + R^{-1}\nabla^2 \mathbf{B}, \qquad \nabla \cdot \mathbf{B} = 0 \tag{1.1}$$

(e.g., Moffatt 1978). Here $\mathbf{u}$ is the fluid flow, of plasma or liquid metal, $\mathbf{B}$ is the magnetic field and R is the magnetic Reynolds number, which is large in many astrophysical environments. The equation (1.1) has been non-dimensionalised using the scale and turn-over time of the flow $\mathbf{u}$. In kinematic dynamo theory the flow $\mathbf{u}$ is fixed; if it is sufficiently complex and R is large enough, the flow may act as a dynamo, giving exponential growth of magnetic energy. For example, for a steady flow $\mathbf{u}$, we will have eigenfunctions of the form

$$\mathbf{B} = \mathbf{b}(x, y, z)e^{(i\omega + p)t}, \tag{1.2}$$

where p is the dynamo growth rate. We shall be concerned with the limit of large magnetic Reynolds number R and in particular 'fast dynamos', for which the largest real growth rate p remains positive and bounded away from zero in this limit. Our interest in this paper is in understanding the role of magnetic helicity within kinematic fast dynamo theory, although in section 5 we give some discussion of nonlinear regimes. The general motivation for the study of fast dynamos is that fast processes, such as the 22-year Solar cycle, are observed in the (nonlinear) Solar dynamo for which $R \sim 10^8$ (e.g., Childress & Gilbert 1995).

In the idealised situation $R = \infty$, in which the fluid is perfectly conducting, magnetic energy will still grow in general, but it is known that the magnetic helicity $H = <\mathbf{A} \cdot \mathbf{B}>$ is conserved (under suitable boundary conditions) as the field evolves, and that this quantity has a topological interpretation (Woltjer 1958, Moffatt 1969). Here $<\cdot>$ is a volume average over the domain occupied by the fluid, and $\mathbf{A}$ is a vector potential for the magnetic field. Plainly for $R = \infty$, if a growing eigenfunction of the form (1.2) can be sensibly defined, it must have zero helicity, as pointed out by Moffatt & Proctor (1985).

This raises the question of what happens to magnetic helicity in the limit when the magnetic Reynolds number is large, but finite, $R \to \infty$. Although the small quantity R^{-1} multiplies the final, diffusive term in (1.1), this term may not generally be neglected, since the field may adopt small scales, and indeed in the Sun much small scale field structure is evident (e.g., Priest 1984). The limit $R \to \infty$ is highly singular and different behaviour may occur for $R = \infty$ and $1 \ll R < \infty$. For example in a kinematic dynamo, a typical flow in the plane amplifies magnetic energy indefinitely for $R = \infty$, but magnetic energy ultimately decays for any finite R, no matter how large, by Cowling's theorem (Cowling 1934, Zeldovich 1957); the onset of the decay is delayed as R is increased.

It is found in MHD, in particular in tokomak and plasma physics, that the ideal helicity invariant tends to be 'robust', being approximately conserved in many situations when the dissipation is present but weak (e.g., Taylor 1974, Berger 1984, Biskamp 1993). This suggests that helicity will be approximately conserved in a dynamo in the limit $R \to \infty$, and so for growing fields the normalised, relative helicity should be small and tend to zero in this limit. Precisely this behaviour is observed by Hughes, Cattaneo & Kim (1996), who discuss the behaviour of magnetic fields in fluid flows with different degrees of flow, or kinetic, helicity, $<\mathbf{u} \cdot \nabla \times \mathbf{u}>$. In each case considered the magnetic helicity falls off with a power law dependence as the magnetic Reynolds number is increased.

The aim of the present paper is to give bounds on the level of helicity in growing magnetic fields, within kinematic dynamo theory, and to discuss its distribution over different scales. We use an exponent defined by Vainshtein & Cattaneo (1992) to give information about the slope of the energy spectrum, and this leads to bounds on the helicity spectrum, related to results of Berger (1984) (see sections 2 and 3). In section 4 we study the magnetic helicity for kinematic dynamo action in a flow first studied by Otani (1993). This gives information not only about the total helicity, but also about its distribution over scales, and we observe considerable cancellation of helicity as it is summed over a range of scales. In particular we observe helicity at the very largest scale having opposite sign to that at smaller scales. To understand how helicity may be distributed over different

scales in a fast dynamo, we consider the idealised 'stretch–twist–fold' picture, in section 5. This makes a link with geometrical ideas of writhe and twist (see Moffatt & Ricca 1992). Finally in section 6 we offer some conclusions.

2. Energy spectrum and Ohmic dissipation

In order to discuss the evolution of helicity in dynamos, there are a number of possible settings we could consider, three-dimensional steady flows, two- or three-dimensional unsteady flows, or even random flows. In order to relate our results most cleanly to the numerical simulations of section 4, we choose to work with a two-dimensional incompressible flow field $\mathbf{u}(x,y,t)$, which has all three components (u_x,u_y,u_z). We take the flow $\mathbf{u}$ to be periodic with period 2π in x and y, and with period T in t. Examples of such flows have been considered by several authors and robust fast dynamos have been obtained (Galloway & Proctor 1992, Otani 1993). Our analysis could be adapted to other situations, and the conclusions would be much the same.

We therefore consider solutions to the induction equation (1.1) (with $\nabla\cdot\mathbf{u}=0$) that are periodic in space. We can define the magnetic energy $E(t)$ by

$$E(t)=\frac{1}{2}<|\mathbf{B}|^2>, \tag{2.1}$$

where $<\cdot>$ represents an average over space. This obeys

$$\partial_t E=-<\mathbf{u}\cdot\mathbf{J}\times\mathbf{B}>-\epsilon<|\mathbf{J}|^2>, \tag{2.2}$$

where $\mathbf{J}=\nabla\times\mathbf{B}$ is the current. Here we have conveniently set $\epsilon=1/R$, so that ϵ is a dimensionless diffusivity and we are interested in the limit of zero diffusion $\epsilon\to 0$.

We suppose that we have integrated the induction equation numerically for the given flow, and the numerical solution is dominated by the fastest growing eigenmode, which here takes the Floquet form

$$\mathbf{B}=e^{(p+i\omega)t+ikz}\mathbf{b}(x,y,t)+\text{c.c.} \tag{2.3}$$

(in the absence of degenerate modes). Here 'c.c.' denotes the complex conjugate of the previous term. The function $\mathbf{b}$ is periodic in t with period T, and p is the real growth rate of the mode with wavenumber $k\neq 0$. The above field is periodic in all three spatial directions, and we take it to lie in a $2\pi\times 2\pi\times 2\pi/k$ box.

The magnetic energy is given by

$$E(t)=e^{2pt}<|\mathbf{b}|^2> \tag{2.4}$$

and grows exponentially in time (superposed on the periodicity inherent in $\mathbf{b}$). Let us factor out the exponential growth and then time average, to define the magnetic energy of the growing eigenfunction as

$$\mathcal{E}=<e^{-2pt}E(t)>_t=<<|\mathbf{b}|^2>>_t, \tag{2.5}$$

where $<\cdot>_t$ denotes a time average. To avoid cumbersome notation we will drop such time-averages from now on, with the understanding that this and similar quadratic quantities are to be time-averaged.

It will be useful to look at the magnetic field in Fourier modes, writing

$$\mathbf{b}(x,y,t) = \sum_{m,n} \mathbf{b}_{mn}(t) e^{imx+iny}. \tag{2.6}$$

In terms of this we have

$$\mathcal{E} = \sum_{m,n} \mathcal{E}_{mn}, \quad \mathcal{E}_{mn} = |\mathbf{b}_{mn}|^2, \tag{2.7}$$

where $\mathcal{E}_{mn}$ is the the contribution to the energy from the (m,n)-mode. We may normalise the eigenfunction so that the contribution from the large-scale field is

$$\mathcal{E}_{\rm LS} \equiv \mathcal{E}_{00} = |\mathbf{b}_{00}|^2 = 1. \tag{2.8}$$

(If this mode is identically zero because of a symmetry, some other large-scale mode may be chosen; the choice is not crucial.) We can also define an energy spectrum $\mathcal{E}(\kappa)$ by

$$\mathcal{E} = \sum_{\kappa=1}^{\infty} \mathcal{E}(\kappa), \quad \mathcal{E}(\kappa) = \sum_{\kappa-1<K(m,n)\le\kappa} |\mathbf{b}_{mn}|^2, \tag{2.9}$$

where $K(m,n) = \sqrt{m^2+n^2+k^2}$ and $\kappa = 1, 2, \ldots$ labels the shells over which the spectrum is computed.

We now introduce fast dynamo scalings. Moffatt & Proctor (1985) show that the diffusive cutoff in a fast dynamo is a length-scale of order $\epsilon^{1/2}$ (see also Galloway & Frisch 1986), and bearing in mind (2.8) above we may postulate an energy spectrum of the form

$$\mathcal{E}(\kappa) \sim \kappa^{2\rho-1}, \quad (1 \lesssim \kappa \lesssim \epsilon^{-1/2}). \tag{2.10}$$

Here $\sim$ is taken to mean 'approximately proportional to', with similar meaning to the inequality symbols $\lesssim$ and $\gtrsim$. Such scalings are consistent with numerical simulations of fast dynamo action (e.g., Childress & Gilbert 1995, section 12.2). With this spectral slope assumed, the total energy is obtained fron integrating (2.10) (and assuming that $\mathcal{E}(\kappa)$ falls rapidly to zero outside the range given),

$$\mathcal{E} \equiv \mathcal{E}/\mathcal{E}_{\rm LS} \sim \begin{cases} 1 & \rho < 0, \\ \epsilon^{-\rho} & \rho > 0, \end{cases} \tag{2.11}$$

and we may identify the exponent ρ with the exponent n of Vainshtein & Cattaneo (1992).†

† Note that for simplicity and brevity we shall here and elsewhere ignore special cases such as $\rho = 0$ in (2.11) which give rise to the logarithmic scaling $\mathcal{E} \sim \log\epsilon$. Such cases are probably only of academic interest and in any case our scaling assumption (2.10) is too crude to make deductions about any variation as weak as $\log\epsilon$.

The global energy balance (2.2) restricts the value of ρ. To see this we first make the key assumption that in a typical fast dynamo all three terms in (2.2) are of similar magnitude, and so

$$\mathcal{E} \sim \epsilon \mathcal{J}, \qquad \mathcal{J} \equiv <|\mathbf{j}|^2>, \tag{2.12}$$

where the constant of proportionality implicit in our use of '$\sim$' depends on the details of the fast dynamo but is independent of ϵ as $\epsilon \to 0$. Here $\mathbf{j}$ is defined for the current $\mathbf{J}$ in a similar way to $\mathbf{b}$ for the magnetic field in (2.3), and in terms of Fourier components (cf. 2.6)

$$\mathbf{j}_{mn} = i\mathbf{K} \times \mathbf{b}_{mn}, \quad (\mathbf{K} \equiv (m, n, k)). \tag{2.13}$$

We may define the spectrum $\mathcal{J}(\kappa)$ of the average current squared, analogously to (2.9), with $\mathcal{J} = <|\mathbf{j}|^2> = \sum_{\kappa=1}^{\infty} \mathcal{J}(\kappa)$. From (2.13,2.10),

$$\mathcal{J}(\kappa) \sim \kappa^{2\rho+1} \qquad (1 \lesssim \kappa \lesssim \epsilon^{-1/2}), \tag{2.14}$$

and so

$$\mathcal{J} \sim \begin{cases} 1 & \rho < -1, \\ \epsilon^{-\rho-1} & \rho > -1 \end{cases} \tag{2.15}$$

(see also Boozer 1992).

Clearly (2.11), (2.12) and (2.15) are only compatible if $\rho \geq 0$, and we will assume this holds in what follows. The limiting case $\rho = 0$ is not ruled out by the above argument, but measurements of ρ in simulations give positive values, as low as 0.25 (Gilbert, Otani & Childress 1993), but increasing for flows of greater complexity (Cattaneo *et al.* 1995); see section 4 below. Therefore we shall take $\rho > 0$ and note that for a typical fast dynamo (in the kinematic regime), the total energy must therefore be dominated by small-scale fields (Vainshtein & Cattaneo 1992). Note that in the two-dimensional case $\rho = 1$ (Vainshtein & Cattaneo 1992); this is not a dynamo, but we observe $\rho \to 1$ (from below) in the two-dimensional limit $k \to 0$ of large-scale dynamo action, in section 4 below. We therefore expect that in typical fast dynamos $0 < \rho < 1$.

It is important to note that there are some examples of fast dynamos which do not fall into our framework. Models such as baker's maps with uniform stretching (Finn & Ott 1988), and that of Arnold *et al.* (1981), amplify magnetic fields without generating fine structure. There is no cascade of magnetic energy to small scales and so (2.10) does not hold; furthermore magnetic dissipation is negligible in (2.2). However these models cannot straightforwardly be embedded as smooth flows in three-dimensional space. For realistic flows, as have been simulated numerically, it is clear that there is a cascade of magnetic energy to small scales (see Galloway & Proctor 1992, Otani 1993, section 4 below), and our framework is correct.

3. Helicity spectrum and dissipation

We now consider the helicity per unit volume given by

$$H(t) = <\mathbf{A} \cdot \mathbf{B}>, \tag{3.1}$$

where $\mathbf{A}$ is the vector potential defined by $\mathbf{B} = \nabla \times \mathbf{A}$, $\nabla \cdot \mathbf{A} = 0$ and $<\mathbf{A}> = 0$. We take there to be no mean field, $<\mathbf{B}> = 0$, this being a dynamo calculation, in which case $\mathbf{A}$ is periodic in space with the same periodicity as $\mathbf{B}$, and may be taken to have Fourier components $\mathbf{a}_{mn}$ (cf. 2.6). The evolution of helicity is governed by

$$\partial_t H = -2\epsilon <\mathbf{B} \cdot \mathbf{J}>. \tag{3.2}$$

If the diffusivity ϵ is strictly zero, then H is a constant, in keeping with its topological interpretation in terms of the linkage of magnetic field lines (Moffatt 1969).

Now suppose we have $0 < \epsilon \ll 1$ and a growing magnetic field eigenmode (2.3). By analogy with the discusion in section 2 above, we may define the helicity of the eigenmode $\mathcal{H} = <\mathbf{a} \cdot \mathbf{b}^* + \mathbf{a}^* \cdot \mathbf{b}>$, its spectrum $\mathcal{H}(\kappa)$, and the contributions $\mathcal{H}_{mn}$ from wavenumber (m, n) in the horizontal. We have $\mathcal{H}_{mn} = \mathbf{a}_{mn} \cdot \mathbf{b}^*_{mn} + \mathbf{a}^*_{mn} \cdot \mathbf{b}_{mn}$ with $\mathbf{a}_{mn} = K^{-2} i\mathbf{K} \times \mathbf{b}_{mn}$. There follows the inequality $|\mathbf{a}_{mn}| \leq K^{-1} |\mathbf{b}_{mn}|$ and so

$$|\mathcal{H}_{mn}| \leq \frac{2}{K(m,n)} \mathcal{E}_{mn}, \quad |\mathcal{H}(\kappa)| \lesssim \frac{2}{\kappa} \mathcal{E}(\kappa). \tag{3.3a,b}$$

The first of these is exact, but the second is approximate, because of the bundling of modes into shells used to define the spectra.

We wish to bound the helicity in a fast dynamo. The most straightforward inequality comes from taking the minimum value, k, of $K(m, n)$ in (3.3a) and summing over all modes, to obtain $|\mathcal{H}| \leq 2\mathcal{E}/k$. This is rather crude, though, as it does not take into account the fact that the energy is predominantly at small scales, where K is much larger than k. To use this fact we substitute (2.10) into (3.3b) and integrate to obtain

$$|\mathcal{H}| \lesssim \begin{cases} 1 & \rho < 1/2, \\ \epsilon^{1/2-\rho} & \rho > 1/2. \end{cases} \tag{3.4}$$

However a tighter bound still may be derived by considering dissipation of helicity according to (3.2) above. We define the current helicity of the eigenmode by $\mathcal{D} = <\mathbf{b} \cdot \mathbf{j}^* + \mathbf{b}^* \cdot \mathbf{j}>$, with contributions $\mathcal{D}_{mn} = \mathbf{b}_{mn} \cdot \mathbf{j}^*_{mn} + \mathbf{b}^*_{mn} \cdot \mathbf{j}_{mn}$. Using $|\mathbf{j}_{mn}| \leq K |\mathbf{b}_{mn}|$ we have that

$$|\mathcal{D}_{mn}| \leq 2K(m,n)\mathcal{E}_{mn}, \quad |\mathcal{D}(\kappa)| \lesssim 2\kappa\mathcal{E}(\kappa) \tag{3.5}$$

and so

$$|\mathcal{D}| \lesssim \epsilon^{-1/2-\rho} \qquad (\rho > 0) \tag{3.6}$$

We then have from (3.2) for the total helicity

$$|\mathcal{H}| \lesssim \epsilon^{1/2-\rho} \qquad (\rho > 0), \tag{3.7}$$

which is tighter than the inequality in (3.4) (for $0 < \rho < 1/2$). This is our main result for the helicity. If the magnetic field is normalised so that the large-scale flux is of order unity, the total energy increases as $\epsilon \to 0$, but the helicity decreases for $\rho < 1/2$ or, for $\rho > 1/2$, increases more slowly than energy, as no more than $\epsilon^{1/2}\mathcal{E}$.

We note that this result may also be obtained by an argument of Berger (1984). Assuming (2.12) holds, we have by the Cauchy–Schwartz inequality and (3.2)

$$(\partial_t H)^2 \leq \epsilon^2 <\mathbf{B}^2><\mathbf{J}^2> \lesssim \epsilon E\, \partial_t E \sim \epsilon \partial_t E^2 \tag{3.8}$$

and so (since growth rates are of order unity),

$$|\mathcal{H}| \lesssim \epsilon^{1/2}\mathcal{E}, \tag{3.9}$$

in agreement with (3.7) above.

Another measure of the helicity in the magnetic field is the relative helicity $\mathcal{H}_R = \mathcal{H}/2\sqrt{<|\mathbf{a}|^2><|\mathbf{b}|^2>}$ of the field, which satisfies $|\mathcal{H}_R| \leq 1$, and is used by Hughes *et al.* (1996). Here, using now familiar arguments,

$$\mathcal{A} \equiv <|\mathbf{a}|^2> \sim \begin{cases} 1 & \rho < 1, \\ \epsilon^{1-\rho} & \rho > 1, \end{cases} \tag{3.10}$$

and so putting this together with (2.11) and (3.7) we have

$$\mathcal{H}_R \lesssim \begin{cases} \epsilon^{(1-\rho)/2} & 0 < \rho < 1, \\ 1 & \rho > 1. \end{cases} \tag{3.11}$$

Assuming that $0 < \rho < 1$ in a typical fast dynamo, $\mathcal{H}_R$ tends to zero in the high-conductivity limit $\epsilon \to 0$.

Hughes *et al.* (1996) also measure the two lengthscales given by

$$l_A = (<|\mathbf{a}|^2>/<|\mathbf{b}|^2>)^{1/2} \sim \begin{cases} \epsilon^{\rho/2} & 0 < \rho < 1, \\ \epsilon^{1/2} & \rho > 1, \end{cases} \tag{3.12}$$

and

$$l_B = (<|\mathbf{b}|^2>/<|\mathbf{j}|^2>)^{1/2} \sim \epsilon^{1/2} \qquad (\rho > 0). \tag{3.13}$$

The same results are obtained by Hughes *et al.* (1996), who give discussion similar to ours. With $0 < \rho < 1$ we may identify the scaling exponents of these authors given by $\mathcal{H}_R \sim \epsilon^{\gamma_1}$, $l_B \sim \epsilon^{\gamma_2}$, $l_A \sim \epsilon^{\gamma_3}$ with $\gamma_1 \geq (1-\rho)/2$, $\gamma_2 = 1/2$ and $\gamma_3 = \rho/2$. We also obtain the inequality $\gamma_1 + \gamma_3 \geq 1/2$, which is satisfied by their numerical results for these flows. Finally note that relative helicity of order unity in a fast dynamo is only possible if $\rho \geq 1$, in which case $l_A, l_B \sim \epsilon^{1/2}$. This is in agreement with the discussion of Moffatt & Proctor (1985), although we know of no numerical examples which show $\rho \geq 1$.

4. Numerical results

We now present some numerical simulations. Our aims are first to confirm the above upper bounds on helicity as $\epsilon \to 0$, and to see how tight these bounds are. Secondly we wish to look in more detail at the distribution of helicity over scales, given by its spectrum $\mathcal{H}(\kappa)$. We study a specific example, the MW+ flow of Otani (1993) given by

$$\mathbf{u}(x,y,t) = 2\cos^2 t(0,\sin x,\cos x) + 2\sin^2 t(\sin y, 0, -\cos y), \tag{4.1}$$

based on modulating two Beltrami waves of positive helicity. Related models involving pulsed Beltrami waves were studied by Bayly & Childress (1988) and related smooth flows by Galloway & Proctor (1992) and Hughes *et al.* (1996). These flows are readily simulated numerically, and we used resolutions of up to 512^2 Fourier modes.

4.1. Fields of moderate scale.

At high $R = 1/\epsilon$ the most unstable magnetic field mode has $k \simeq 0.8$ and shows structure over a range of scales; its growth rate is $p \simeq 0.393$ for small ϵ. We first investigate the behaviour of helicity and energy in this case.

Figure 1 shows the scaling of $\mathcal{E}$ (triangles), $\mathcal{J}$ (pluses) and $|\mathcal{H}|$ (crosses) as functions of $1/\epsilon$ on a log-log plot. The scaling of $\mathcal{E}$ is very clear: the straight line observed gives the value $\rho \simeq 0.25$ as obtained by Gilbert, Otani & Childress (1993). The scaling for the current $\mathcal{J}$ is less clear; the best estimate of the slope for the smallest values of ϵ would give $\rho \simeq 0.18$, but the graph has some upward curvature. In measuring the current the dissipation scale is more heavily weighted than for the energy, leading to slower convergence to the scaling law as $\epsilon \to 0$. For a given ϵ higher numerical resolutions are also required to obtain the data point on the $\mathcal{J}$ curve accurately, than for $\mathcal{E}$. We therefore use the $\mathcal{E}$ scaling to estimate $\rho \simeq 0.25$.

This implies from (3.7) that the total helicity $\mathcal{H}$ must fall off at least as fast as $\epsilon^{0.25}$. This slope is shown by the dashed line in figure 1 and it may be seen that the total helicity falls off faster than this upper bound requires, more as $\epsilon^{0.5}$, with some downward curvature. To confirm the connection with the energy spectrum, figure 2(a) shows $\mathcal{E}(\kappa)$ plotted for several values of ϵ. The spectral slope shows reasonable agreement with $\mathcal{E}(\kappa) \sim \kappa^{-0.50}$ (shown dashed) as suggested theoretically, but is rather noisy, despite time averaging over one period.

Although the total helicity goes to zero with ϵ, examination of $\mathcal{H}(\kappa)$ shows that this arises from significant cancellation of positive and negative helicity at different scales. Figure 2(b) shows the logarithm of $|\mathcal{H}(\kappa)|$. In order to show its sign and yet use a log-log graph we in fact plot $f(\mathcal{H}(\kappa))$ against $\log_{10}\kappa$, where

$$f(x) = \mathrm{sign}(x)\log_{10}(\max(1, 10^6 x)). \tag{4.2}$$

Thus positive values of helicity appear on the graph on the range 0 to 6, and negative values on the range -6 to 0. Also shown by dashed lines are the bounds (for $1/\epsilon = 10^5$)

obtained from summing (3.3a) over all the modes in the calculation. At the very largest scale, when $\kappa = 1$ and only the large-scale $\mathbf{b}_{00}$ mode is included in the spectral sum, the helicity is significant, and negative with $\mathcal{H}_{00} \simeq -1.5$ for small ϵ. We see that although the total helicity goes to zero even faster than our bounds indicate, this is not much of a constraint on the magnetic field at large scales. The large scale modes generated in the growing field can have significant helicity, here negative, while helicity of the opposite sign is spread out along the cascade to small scales, the total helicity being negligibly small as $\epsilon \to 0$.

4.2. Large-scale fields.

In the above example we took $k = 0.8$, giving the fastest growing mode in which the scale of the magnetic field is comparable with that of the fluid flow. Also of interest is the behaviour of large-scale fields with small values of k. Although these have smaller growth rates, tending to zero as $k \to 0$, study of these modes gives insight into the mean-field dynamo regime. Therefore, as a further example, we consider Otani's MW+ flow (4.1) with $k = 0.05$ and $k = 0.01$. Growth rates are shown in figure 3(a), and it may be seen that these saturate rather slowly as $\epsilon \to 0$. Figures 3(b,c) are similar to figure 1 and show $\mathcal{E}$ (triangles) and $|\mathcal{H}|$ (crosses) plotted against $1/\epsilon$ in a log–log plot ($\mathcal{J}$ is not shown); in figure 3(b) $k = 0.05$ while in 3(c) $k = 0.01$. Here the power law for energy is steeper and takes longer to become established as $\epsilon \to 0$. Measurements of the exponent ρ give $\rho \simeq 0.60$ for $k = 0.05$ (using the range $500 \le 1/\epsilon \le 10^4$) and $\rho \simeq 0.72$ for $k = 0.01$ (using $10^3 \le 1/\epsilon \le 10^4$). The upper bounds on the helicity are $\epsilon^{-0.10}$ and $\epsilon^{-0.22}$ respectively, shown dashed, and the actual helicity lies well within these bounds, decaying rather than growing.

We note that the value of ρ appears to increase as k is reduced, corresponding to more energy in the small scales. With a field of larger scale in the z-direction, we approach the situation where the field is independent of z, and the arguments of Vainshtein & Cattaneo (1992) come into play, which predict $\rho = 1$ for the non-dynamo case $k = 0$, from consideration of the vector potential for the field. The energy spectrum is flatter, and the helicity spectrum shows greater fluctuations than for $k = 0.8$ (we do not plot either of these here). There is strong negative helicity at the largest scale and positive helicity further down the spectrum.

5. Helicity in the stretch–twist–fold picture

We have seen that in Otani's flow there is significant helicity at the largest scale, balanced by opposite helicity at smaller scales, to give a total helicity that is vanishingly small in the fast dynamo limit $\epsilon \to 0$. In this section we consider the behaviour of helicity and its distribution in the original stretch–twist–fold (STF) fast dynamo picture of Vainshtein & Zeldovich (1972). Although the STF dynamo is only a picture, raises many questions, and indeed is difficult to realise numerically (see Vainshtein *et al.* 1996, Vainshtein, Sagdeev & Rosner 1997), it remains an important guide to intuition. Our aims here are to understand how helicity is distributed over scales in a fast dynamo with a helical flow field, and to

give indications of how this is modified in a dynamical regime in which the Lorentz force becomes important.

Figure 4 shows the basic STF process on a tube of flux (Vainshtein & Zeldovich 1972). We note that the flow field as depicted by the bold arrows itself has a positive sense of kinetic helicity, measured by $\mathbf{u} \cdot \nabla \times \mathbf{u}$, as in a basic 'cyclonic event' of Parker (1955). We take the helicity of the magnetic field in figure 4(a) to be $H = 0$, for example by taking the field lines to be circular and unlinked. We also take the flux of the tube to be $\Phi = 1$ and the fluid to be perfectly conducting, $\epsilon = 0$, so that the magnetic field line topology is preserved subsequently. Thus in 4(d) the helicity remains zero, but we may identify two, cancelling contributions as follows. To do this we use Moffatt & Ricca (1992) in the rest of this section; this paper should be consulted for further discussion, references and historical perspective.

The first contribution to the helicity comes from considering the centre line of the tube; initially this is just a circle C_0, but is depicted after the stretch–twist operations in figure 5(a), and as the curve C_1 after after one complete STF operation in figure 5(b). When deformed to lie almost in a plane, C_1 (nearly) crosses itself just once. If we associate an integer ± 1 with the crossing according to its sense as also shown in figure 5(a), we obtain that the 'writhe' of C_1 is -1 and this gives a 'writhe contribution' to the helicity of $H_{\mathrm{wr}} = -1$. More generally the writhe of any curve C is given by the integral

$$\mathrm{W}(C) = \frac{1}{4\pi} \oint_C \oint_C \frac{d\mathbf{r} \times d\mathbf{r}' \cdot (\mathbf{r} - \mathbf{r}')}{r^3}. \tag{5.1}$$

There is a compensating 'twist' of field lines inside the tube: relative to the tube's centre line (or more precisely a Serret–Frenet framing of the curve C_1) the field lines rotate through an angle 2π when the centre line is traversed once (Moffatt & Proctor 1985). This gives a 'twist' of $+1$, and the 'twist contribution' to the helicity is $H_{\mathrm{tw}} = +1$. The total helicity after one STF step is $H = H_{\mathrm{wr}} + H_{\mathrm{tw}} = 0$.

Although the two forms of helicity sum to zero, they are associated with different scales of the field. The positive twist helicity is associated with structure internal to the tube, whereas the negative writhe helicity is related to the twisting of the pair of tubes about each other. Thus the STF process has generated positive helicity at the smallest scale, and negative helicity at a slightly larger scale. This transfer, of negative magnetic helicity to larger scale, and positive to smaller scale, in a flow field with positive kinetic helicity, is well known (see, e.g., Moffatt 1978, Pouquet, Frisch & Léorat 1976, Brandenburg 2001).

Now consider applying the stretch–twist (figure 5(c)) and fold (figure 5(d)) operations a second time; the center line C_2 of the tube is shown. This time the stretch–twist of a pair of flux tubes gives a writhe of -4 as pairs of 2 tubes cross each other. However at the same time two individual tubes wrap around each other and this gives another contribution to the writhe of $+2$ as shown. Again we may consider the writhe as distributed over different scales. On the largest scale involving $4 = 2^2$ tubes, there is a writhe of $H_{\mathrm{wr2}} = -4$. On the next scale, involving $2 = 2^1$ tubes, there is a writhe of $H_{\mathrm{wr1}} = 2 - 1 = 1$. The total writhe is then $H_{\mathrm{wr}} = H_{\mathrm{wr1}} + H_{\mathrm{wr2}} = -3$ and so the corresponding twist is $H_{\mathrm{tw}} = 3$ to compensate.

The general picture now becomes clear. After the step $n-1$ of the STF process we have 2^{n-1} tubes of field with centre line C_{n-1}. We then do the stretch–twist–fold operation. This generates a bundle of 2^n tubes of flux with centre line C_n. Associated with the fold operation is positive and negative writhe. The negative writhe is on the largest scale, involving all 2^n tubes, and corresponds to 2^{n-1} tubes crossing over 2^{n-1} tubes and is $-2^{n-1}\times 2^{n-1} = -2^{2n-2}$ (figure 5(e)). The positive writhe is on the next scale down, involving 2^{n-1} tubes being twisted through 2π, and gives a writhe of $2^{n-1}(2^{n-1}-1)$ (figure 5(f)). If after n steps we let $H_{\mathrm{wr}\,j}$ denote the writhe that involves 2^j tubes we have for the largest scale

$$H_{\mathrm{wr}\,n} = -2^{2n-2} \qquad (j=n), \tag{5.2}$$

while for smaller scales,

$$H_{\mathrm{wr}\,j} = -2^{2j-2} + 2^j(2^j-1) \qquad (j=1,2,\ldots,n-1). \tag{5.3}$$

In (5.3) the negative writhe is generated at step j, and the positive writhe at step $j+1$. The total writhe involving 2^j tubes is

$$H_{\mathrm{wr}\,j} = 2^{j-1}(3\times 2^{j-1}-2) \qquad (j=1,2,\ldots,n-1). \tag{5.4}$$

The total twist helicity is $H_{\mathrm{tw}} = 2^n - 1$, given by the field structure internal to the tubes.

Although the STF picture is very idealised, it does throw light on the numerical results and their relation with the analysis of sections 2 and 3. First, we observe the same structure to the helicity spectrum, with negative helicity at the largest scale, and positive helicity at all smaller scales. Second, we note that the net positive writhe at a given intermediate scale comes from a positive and a negative contribution, which we have been careful to isolate above in (5.3). Kinematically there is no reason why the positive and negative contributions, for example the $+2$ and -1 shown in figure 5(d), should cancel other than fortuitously. This agrees with the numerical results that indicate that the inequality $|\mathcal{H}(\kappa)| \lesssim 2\mathcal{E}(\kappa)/\kappa$ is not well saturated in simulations (see figure 2(b)); there is more energy at a given scale than is required by the total helicity at that scale. Finally if weak diffusion $\epsilon > 0$ is now introduced, obviously the tubes of field will start to reconnect when they reach scales of order $\epsilon^{1/2}$. The twist helicity will be destroyed first, and then writhe $H_{\mathrm{wr}\,j}$ for increasing j. The total helicity will be negative and small.

The above picture, although crude, also gives some indications about what may occur initially when Lorentz forces become important. Let us consider the case when the fluid Reynolds number is of a similar size to the magnetic Reynolds number for simplicity. It is clear, looking at figure 5(d), that it is energetically favourable for the $+2$ writhe and the -1 writhe now to cancel by the interchange of sections of field lines. This would immediately reduce the energy while preserving the field line topology at this scale. Similarly the plus and minus contributions (5.3) to the writhe at a given scale may be partially cancelled by interchange motions. Thus we may expect that at the onset of dynamical effects the total number of crossings of the magnetic field will be reduced by dynamical, magnetic relaxation effects (Moffatt 1985). The 'crossing number' of a continuous vector field has

been defined by Freedman & He (1991) (see also Berger 1993) as

$$C(\mathbf{B}) = \frac{1}{4\pi} \int \int \frac{|\mathbf{B}(\mathbf{r}) \times \mathbf{B}(\mathbf{r}') \cdot (\mathbf{r} - \mathbf{r}')|}{|\mathbf{r} - \mathbf{r}'|^3} \, d^3\mathbf{r} \, d^3\mathbf{r}'. \tag{5.5}$$

This definition is analogous to (5.1) for a continuous field, but with the absolute value of the integrand taken. We may expect that this quantity decreases significantly at the onset of saturation, while plus and minus writhe cancel through interchange motions. This also suggests that the upper bound $|\mathcal{H}(\kappa)| \lesssim 2\mathcal{E}(\kappa)/\kappa$ will be quite closely attained after equilibration, and this is in fact seen in numerical simulations (Brandenburg 2001).

6. Discussion

We have discussed the role of helicity in kinematic dynamos for the astrophysically important limit of large magnetic Reynolds number R. We have focussed on fast dynamos, in which the growth rates remain of order the turn-over time-scale in this limit. Hughes *et al.* (1996) showed that the relative magnetic helicity goes to zero as $R \to \infty$ in a growing field, and we have derived an upper bound on the helicity, relating it to the slope of the energy spectrum. Studying the distribution of helicity over different scales revealed however that there is a great deal of cancellation: in the examples we considered there was strong negative helicity at the largest scale, almost entirely cancelled by positive helicity at moderate and small scales. A similar behaviour was seen in the idealised STF picture of a fast dynamo, and some predictions were made of behaviour at the onset of saturation, when Lorentz tension forces come into play.

The flow fields we have used have maximal kinetic helicity $\mathbf{u} \cdot \nabla \times \mathbf{u}$. Hughes *et al.* (1996) study a number of dynamo flows which have zero kinetic helicity and it would be interesting to consider the role of magnetic helicity in these dynamos in more detail. Obviously the inequalities we have derived remain correct as they use no information about the flow field. However the distribution of magnetic helicity over the different scales will probably be less coherent in fast dynamos with zero kinetic helicity.

Our study may be summarised by saying that the exact conservation of helicity in ideal MHD is replaced by very low levels of total helicity at large R in a kinematic fast dynamo. However this low total helicity does not seem to act as a constraint on field growth nor on the helicity of the large-scale field. In our example we have seen a strongly helical field on the large scale, with smaller scales containing cancelling helicity of the opposite sign. At first sight this stands in contrast to recent ideas of Brandenburg (2001) (see also Vishniac & Cho 2000), who argues that in nonlinear, high-R dynamos helicity 'drives' the large-scale field. These arguments are based on conservation of helicity, the fact that the large-scale fields are strongly helical, and that dissipation of helicity is small. It is certainly true that non-linear dynamos with helical and non-helical forcing of the velocity field show very different behaviour of the large-scale fields (e.g., Pouquet *et al.* 1976, Maksymczuk & Gilbert 1999). There is no direct contradiction with our kinematic results above, since the elastic nature of Lorentz forces may be such as to minimize energy for a given helicity at

each scale, and so in that sense helicity may control large-scale fields. However the matter is clearly delicate since helicity may take either sign and cancel, and so dissipation of total helicity is not a clear guide to the evolution of helicity at large scales.

On this note, the following numerical simulation might be of interest to determine cause and effect: to what extent dissipation of helicity drives the large-scale field, or to what extent it passively follows. A nonlinear run (1) could be started using a velocity forcing with positive helicity and run up to time $t = T$. In another run (2) the forcing would have positive helicity for $0 \leq t \leq T/2$ but negative for $T/2 \leq t \leq T$. There are then two possible outcomes for the second run. First, the field may take a significant time to adjust after $t = T/2$ and to reverse its magnetic helicity at large scales. During this adjustment period we would expect to see a decay of magnetic energy and halting of any inverse cascade (see Pouquet *et al.* 1976, Gilbert & Sulem 1990). If this long adjustment occurs (and its length increases for $R \to \infty$) before the evolution resumes as the mirror image of run (1), we may conclude the large-scale field is controlled by dissipation of helicity. The second possibility is that the large-scale fields adjust rapidly at $t = T/2$ and change sign of helicity (in a fashion independent of R for large R), this change being taken up by the helicity at lower scales. During the transition the magnetic energy would not be diminished significantly, and the inverse cascade would be only interrupted briefly. If this is the case then it will be clear that helicity is playing a minor role in driving the nonlinear dynamo.

Acknowledgements

I am grateful to Axel Brandenburg, Mitch Berger, Steve Childress, Keith Moffatt, Mike Proctor and Renzo Ricca for useful discussions and helpful references. This work was undertaken at the Geometry and Topology of Fluid Flow programme at the Isaac Newton Institute of Mathematical Sciences in Cambridge. I would like to thank the organisers and staff for a very fruitful programme. Large numerical runs were performed on the University of Exeter IBM SP/3 supercomputer, suported by the HEFCE JREI.

Figure captions

Figure 1. $\log_{10} \mathcal{E}$ (triangles), $\log_{10} \mathcal{J}$ (pluses) and $\log_{10} |\mathcal{H}|$ (crosses) are plotted against $\log_{10} 1/\epsilon$, for Otani's flow with $k = 0.8$. The dashed line indicates a power law dependence of $\epsilon^{0.25}$.

Figure 2. (a) $\log_{10} \mathcal{E}(\kappa)$ (b) $f(\mathcal{H}(\kappa))$, plotted against $\log_{10} \kappa$ for $1/\epsilon = 10, 20, 50, \ldots 10^5$. In (a) the dashed line indicates a power law dependence $\kappa^{-0.5}$. In (b) the dashed lines show the upper and lower bounds obtained from (3.3a).

Figure 3. (a) Growth rate p plotted against $\log_{10} 1/\epsilon$ for Otani's flow with $k = 0.05$ (upper curve), $k = 0.01$ (lower curve). (b,c) $\log_{10} \mathcal{E}$ (triangles) and $\log_{10} |\mathcal{H}|$ (crosses) are plotted against $\log_{10} 1/\epsilon$, for Otani's flow with (b) $k = 0.05$ and (c) $k = 0.01$. The dashed lines indicate a power law dependence of (b) $\epsilon^{-0.10}$ and (c) $\epsilon^{-0.22}$.

Figure 4. The stretch–twist–fold process: an initial flux tube (a), is stretched (b), twisted (c) and folded (d), to obtain a doubled flux tube.

Figure 5. The center line of the flux tube after (a,b) one and (c,d) two iterations of the stretch–twist–fold process. Contributions to the total writhe of the curve (with sign convention shown in (a)) are marked near each set of crossings. The writhe generated at the nth iteration is shown as (e) the negative contribution, (f) the positive contribution.

References

Arnold, V.I., Zeldovich, Ya.B., Ruzmaikin, A.A. & Sokoloff, D.D. 1981 *Zh. Eksp. Teor. Fiz.* **81**, 2052–2058. [English transl.: *Sov. Phys. JETP* **54** (1981) 1083–1086.]

Bayly, B.J. & Childress, S. 1988 *Geophys. Astrophys. Fluid Dyn.* **44**, 211–240.

Berger, M.A. 1984 *Geophys. Astrophys. Fluid Dyn.* **30**, 79–104.

Berger, M.A. 1993 *Phys. Rev. Lett.* **70**, 705–708.

Biskamp, D. 1993 *Nonlinear Magnetohydrodynamics.* Cambridge University Press.

Boozer, A.H. 1992 *Astrophys. J.* **394**, 357–362.

Brandenburg, A. 2001 The inverse cascade and nonlinear alpha-effect in simulations of isotropic helical hydromagnetic turbulence. *Astrophys. J.* **550**, to appear.

Cattaneo, F., Kim, E., Proctor, M.R.E. & Tao, L. 1995 *Phys. Rev. Lett.* **75**, 1522–1525

Childress, S. & Gilbert, A.D. 1995 *Stretch, Twist, Fold: The Fast Dynamo.* Springer Verlag.

Cowling, T.G. 1934 *Mon. Not. Roy. Astr. Soc.* **140**, 39–48.

Finn, J.M. & Ott, E. 1988 *Phys. Fluids* **31**, 2992–3011.

Freedman, M.H. & He, Z.-X. 1991 *Ann. Math.* **134**, 189–229.

Galloway, D.J. & Frisch, U. 1986 *Geophys. Astrophys. Fluid Dyn.* **36**, 53–83.

Galloway, D.J. & Proctor, M.R.E. 1992 *Nature* **356**, 691–693.

Gilbert, A.D., Otani, N.F. & Childress, S. 1993 In *Solar and Planetary Dynamos* (ed. M.R.E. Proctor, P.C. Matthews, A.M. Rucklidge), pp. 129–136. Cambridge University Press.

Hughes, D.W., Cattaneo, F. & Kim, E.J. 1996 *Phys. Lett. A* **223**, 167–172.

Maksymczuk, J. & Gilbert, A.D. 1999 In *Stellar Dynamos: Nonlinearity and Chaotic Flows* (ed. M. Núñez & A. Ferriz-Mas), pp. 97–106. ASP Conf. Series, vol. 178.

Moffatt, H.K. 1969 *J. Fluid Mech.* **35**, 117–129.

Moffatt, H.K. 1978 *Magnetic Field Generation in Electrically Conducting Fluids.* Cambridge University Press.

Moffatt, H.K. 1985 *J. Fluid Mech.* **159**, 359–378.

Moffatt, H.K. & Proctor, M.R.E. 1985 *J. Fluid Mech.* **154**, 493–507.

Moffatt, H.K. & Ricca, R.L. 1992 *Proc. R. Soc. Lond. A* **439**, 411–429.

Otani, N.F. 1993 *J. Fluid Mech.* **253**, 327–340.

Parker, E.N. 1955 *Astrophys. J.* **122**, 293–314.

Pouquet, A., Frisch, U. & Léorat, J. 1976 *J. Fluid Mech.* **77**, 321–354.

Priest, E.R. 1984 *Solar Magnetohydrodynamics.* Reidel Publishing Company.

Taylor, J.B. 1974 *Phys. Rev. Lett.* **33**, 1139–1141.

Vainshtein, S.I. & Cattaneo, F. 1992 *Astrophys. J.* **393**, 199–203.

Vainshtein, S.I. & Zeldovich, Ya.B. 1972 *Usp. Fiz. Nauk* **106**, 431–457. [English transl.: *Sov. Phys. Usp.* **15** (1972), 159–172.]

Vainshtein, S.I., Sagdeev, R.Z., Rosner, R. & Kim, E.-J. 1996 *Phys. Rev. E*, **53** 4729–4744.

Vainshtein, S.I., Sagdeev, R.Z. & Rosner, R. 1997 *Phys. Rev. E*, **56** 1605–1622.

Vishniac, E.T. & Cho, J. 2000 Magnetic helicity conservation and astrophysical dynamos. Preprint.

Woltjer, L. 1958 *Proc. Nat. Acad. Sci. USA* **44**, 489–491.

Zeldovich, Ya.B. 1957 *Sov. Phys. JETP* **4**, 460–462.

FIGURE 1

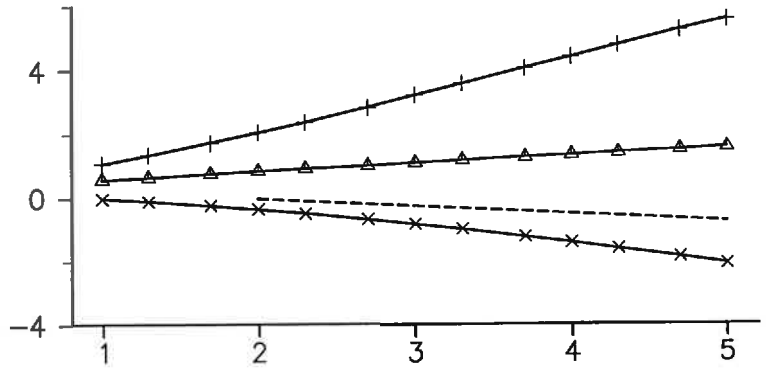

FIGURE (2)

(a)

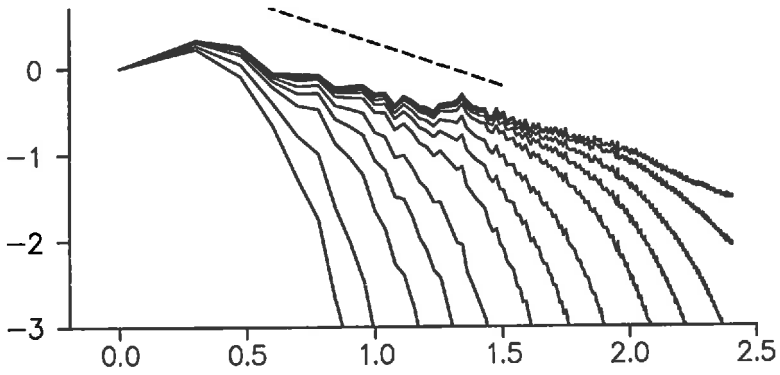

(b)

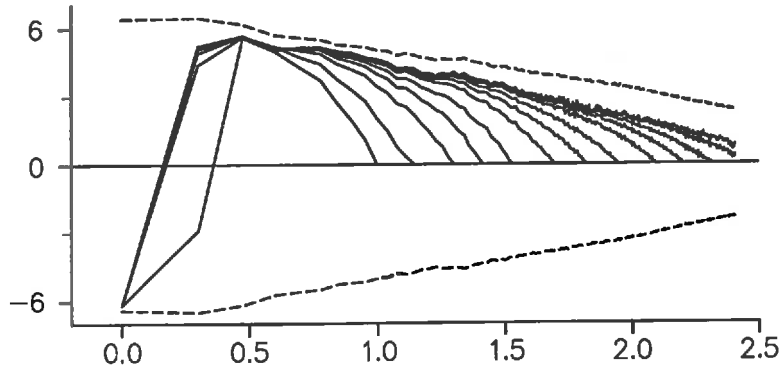

FIGURE 3

(a)

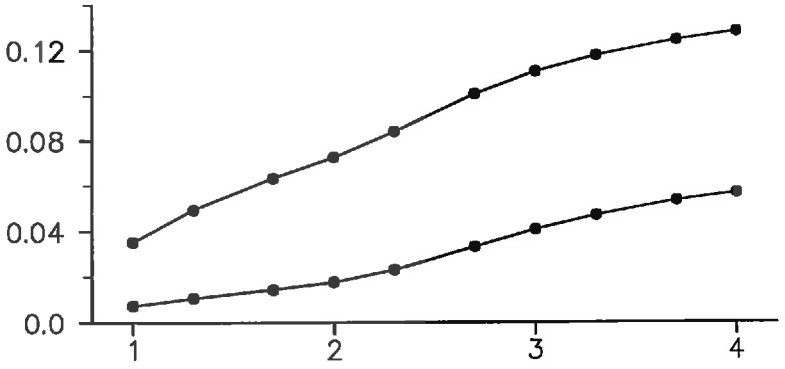

(b)

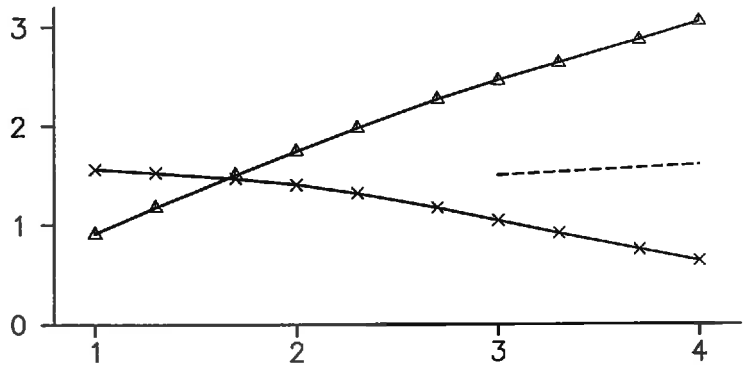

(c)

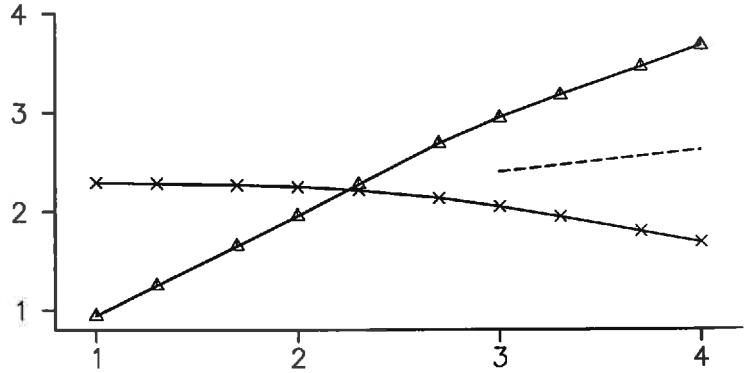

Figure 4

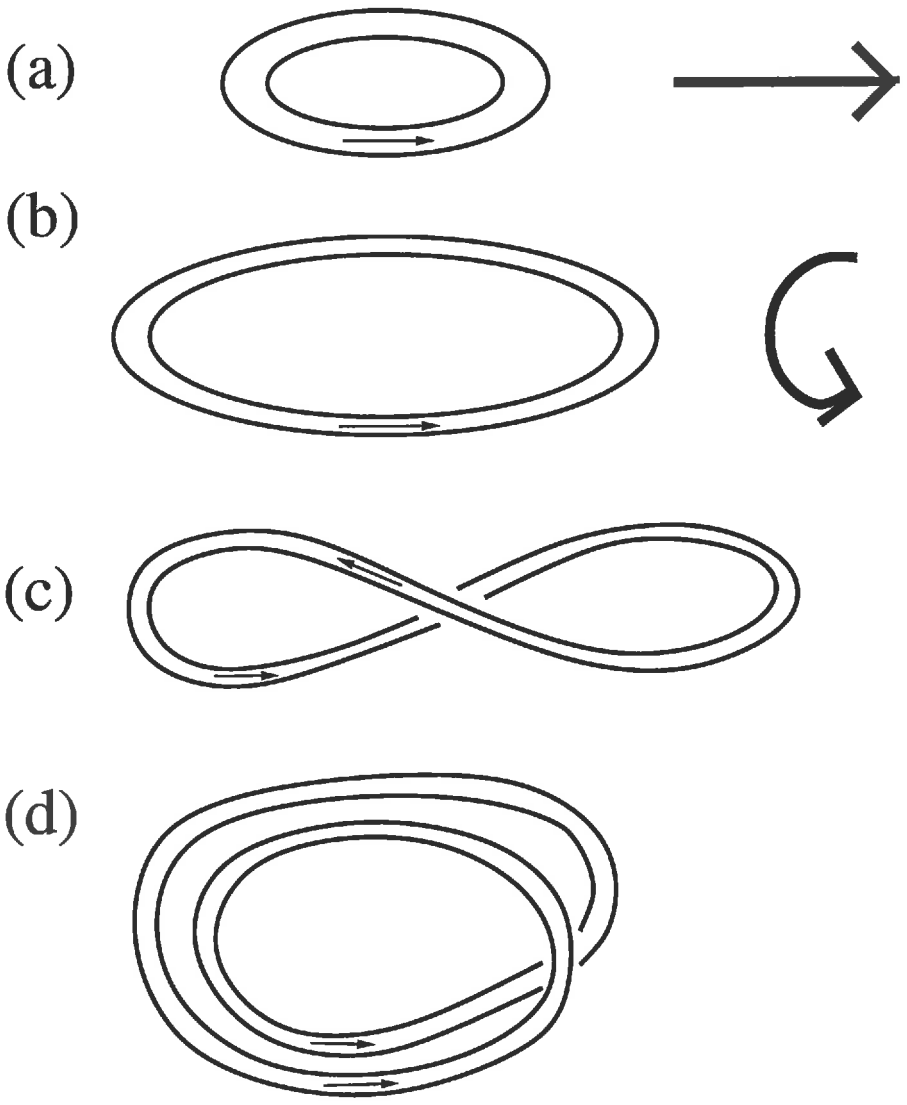

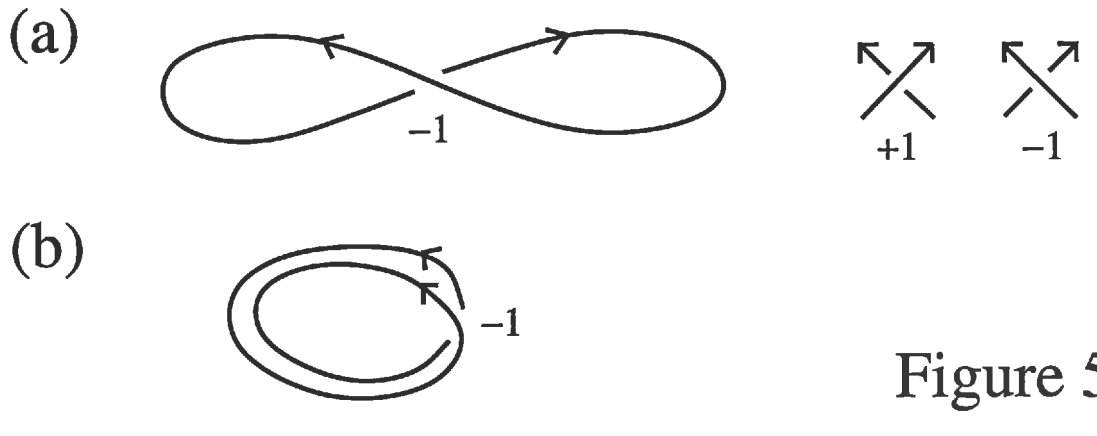

Figure 5